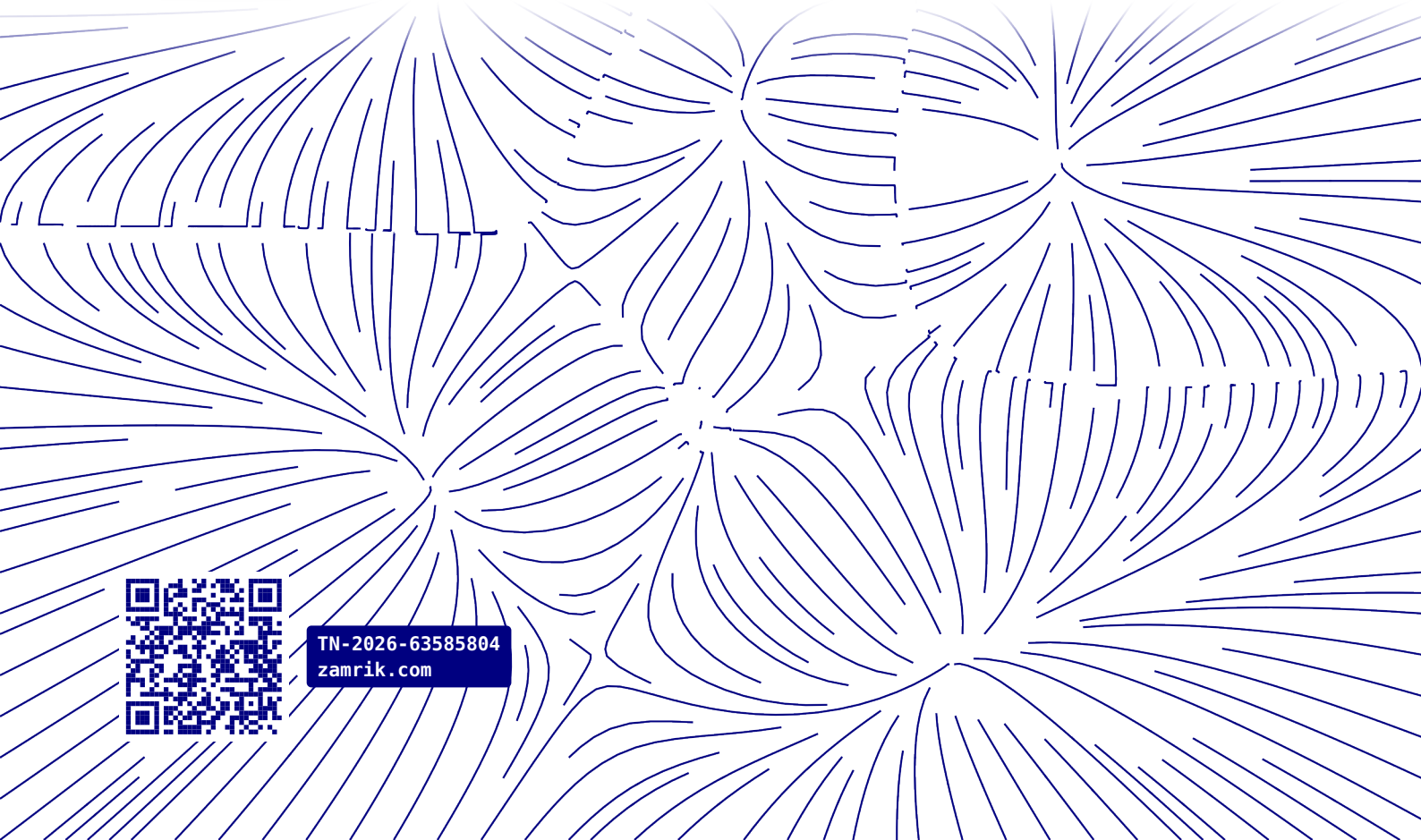
TECHNICAL NOTE

Euler Error for Brownian Motion with Dry Friction

Supervised by Dr. T. Zamrik

31-AUG-2026

Gradient flow of the Peaks function: $\dot{\mathbf{x}} = \nabla f(\mathbf{x}), \quad f(x,y) = \left|3(1-x)^2 e^{-x^2-(y+1)^2} - 10(x/5 - x^3 - y^5)e^{-x^2-y^2} - \frac{1}{3}e^{-(x+1)^2-y^2}\right|$



TN-2026-63585804
zamrik.com



Zamrik Quant Research

The research arm of Zamrik Quant Lab

Copyright

© 2026 T. Zamrik. All rights reserved. Published by Zamrik Quant Research. No part of this document may be reproduced, stored, distributed or adapted, in whole or in part, by any means, without the prior written permission of the publisher, except for brief quotation with full citation. Requests for permission: info@zamrik.com.

Suggested Citation

Stochastic Analysis Desk, Zamrik Quant Research (2026). 'Euler Error for Brownian Motion with Dry Friction'. *Zamrik Quant Research Technical Note* **TN-2026-63585804**. Available at https://zamrik.com/research-items/tn-2026-63585804/.

About Zamrik Quant Research

Zamrik Quant Research is the research arm of Zamrik Quant Lab. It works through five research desks, from market microstructure and derivatives to optimal control, stochastic analysis and applied mathematics, and publishes everything it finds in the open: research papers, notebooks that run on Kaggle, free tools that answer one practical question, and essays.

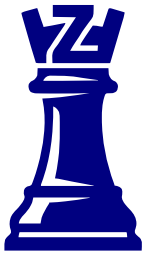
The five desks are Market Microstructure & Trading; Derivatives & Volatility; Optimal Control & Decision; Stochastic Analysis; and Applied Mathematics. Each paper, notebook, tool and essay belongs to exactly one desk. Zamrik Quant Research is run by a small, independent team, headed by Dr. T. Zamrik. We are self-funded: no sponsors, no advertisers, no outside capital.

Every publication passes through the same five functions before anyone outside sees it: research, data, software, verification and production. We never retrofit the mathematics to a conclusion chosen in advance. Every number is checked two independent ways. Every figure is re-run from its code. When we find an error, or replace a piece with a better one, we record it in the public corrections log at https://zamrik.com/corrections/.

Legal Notice

This note is research and education. Nothing in it is investment, financial, legal or engineering advice; nothing is a recommendation to buy or sell shares of stock, derivative contracts, bonds, or any other instrument or property; and nothing is a forecast. You are responsible for your own decisions. Figures and code are provided as they are. Care and independent checks reduce errors but cannot rule them out, so no warranty is given. The views expressed are those of the Stochastic Analysis Desk.

STOCHASTIC ANALYSIS DESK ZAMRIK QUANT RESEARCH



TECHNICAL NOTE

Euler Error for Brownian Motion with Dry Friction

Supervised by Dr. T. Zamrik[1]

31-AUG-2026 TN-2026-63585804

Abstract. We study the continuous Euler approximation of the scalar diffusion with inward sign drift and constant nonzero diffusion coefficient. At mesh size h, the error scaled by $h^{-3/4}$ converges stably in the uniform topology to a conditionally Gaussian process driven by local time at the discontinuity. The drift feeds the error back through the same local time, producing an explicitly solvable linear equation. A bounded Brownian corrector gives the forcing variance directly as $-\sqrt{2/\pi}\,\zeta(-1/2)$. A shrinking-band occupation argument accommodates the endogenous Euler error, and uniform moments justify convergence of the mean-square error. The terminal constant is expressed using the normal distribution function for every deterministic initial value. For the pure dry-friction interpretation, the result gives an asymptotic time-step prescription for a specified velocity error. Coupled simulations illustrate its finite-grid performance and retain both sampling uncertainty and reference-grid sensitivity.

TN-2026-63585804 · Stochastic Analysis Desk · Technical Note · Published 31-AUG-2026 · Reading time: about 16 min

1. Introduction

A discontinuity in the restoring force changes both the rate and the structure of Euler error. For the equation $dX_t = -a\,\mathrm{sgn}(X_t)dt + \sigma dW_t$, the drift reverses at zero, so visits near that point determine the leading discretisation error. The same equation describes velocity under dry friction and Gaussian white-noise forcing [8]. The practical question is how accurately a uniform-step simulation follows the velocity trajectory driven by the same noise.

The rate alone is not the contribution sought here. Neuenkirch and Szölgyenyi [1] connect irregular-drift Euler error to quadrature, obtaining convergence bounds. Müller-Gronbach and Yaroslavtseva [2] establish a 3/4 lower-bound mechanism for discontinuous drift; Ellinger [3] treats piecewise Lipschitz drifts without the earlier monotonicity restriction. These results place a sharp constraint on what a nonadaptive approximation can achieve. The present result identifies the limiting Euler error and its constant for the inward sign model.

Dareiotis, Gerencsér and Lê [4] prove an irregular-drift central limit theorem at square-

[1]Correspondence: Stochastic Analysis Desk, Zamrik Quant Research, info@zamrik.com.

root scaling. The displayed forcing in their limit equation vanishes for constant diffusion; applying their coefficient assumptions to the sign model would additionally require localisation. That theorem therefore does not directly supply the finer-scale limit derived here. Jacod's occupation theorem [5] and conditional-Gaussian martingale theorem [6] supply the two external limit results used in our proof. Occupation approximation constants are also studied by Altmeyer and Le Guével [7]; we calculate the constant needed here directly, fixing the indicator and local-time conventions throughout.

The proof has two distinct scales. The Brownian corrector acts in a band of width $h^{1/2}$, whereas the drift feedback is determined by the narrower, random band of width $h^{3/4}$. Establishing tightness before inserting this random band avoids a circular linearisation. The application follows the numerical cautions emphasized by Göttlich, Lux and Neuenkirch [9]: a fine Euler reference remains an approximation, and a visible rate does not establish an exact error constant.

Main findings

- We prove a functional stable limit theorem for Euler error, with a Brownian forcing term indexed by local time and a damping term integrated against local time.
- The proof constructs a bounded Brownian corrector and establishes a shrinking-band occupation lemma whose random thresholds may depend on the Euler error; this identifies the local-time feedback without assuming independence.
- The forcing constant is $c = -\sqrt{2/\pi}\,\zeta(-1/2)$, obtained from an explicit Fourier calculation.
- Uniform bounds for every finite moment yield convergence of the scaled terminal mean-square error to a closed expression for all deterministic starting points.
- In two dimensionless dry-friction regimes, the saved coupling experiment quantifies the finite-grid accuracy of the resulting mesh prescription.

2. Setting and main theorem

Definition 1 (Scheme and local-time convention)**.** Fix $a, \sigma, T > 0$ and a deterministic $x_0 \in \mathbb{R}$. Let

$$dX_t = -a\,\mathrm{sgn}(X_t)\,dt + \sigma\,dW_t, \qquad X_0 = x_0, \tag{2.1}$$

where $\mathrm{sgn}(0) = 0$. Let $h = T/n$, $\eta_h(t) = h\lfloor t/h \rfloor$, and use the continuous Euler interpolation driven by the same Brownian motion:

$$X_t^h = x_0 - a\int_0^t \mathrm{sgn}(X_{\eta_h(s)}^h)\,ds + \sigma W_t. \tag{2.2}$$

The local time $L_t = L_t^0(X)$ is the symmetric semimartingale local time, so

$$|X_t| = |x_0| + \int_0^t \mathrm{sgn}(X_s)\,dX_s + L_t, \qquad \int_0^t f(X_s)\sigma^2\,ds = \int_{\mathbb{R}} f(y)L_t^y(X)\,dy. \tag{2.3}$$

Theorem 1 (Stable Euler limit)**.** Under Definition 1, put $c = -\sqrt{2/\pi}\,\zeta(-1/2) > 0$. In $C([0,T])$, stably with respect to the Brownian path,

$$h^{-3/4}(X - X^h) \implies_{\mathrm{st}} U, \tag{2.4}$$

where, on an extension carrying a Brownian motion B' independent of the original path, U is the unique continuous solution of

$$U_t = -\frac{2a}{\sigma^2}\int_0^t U_s\, dL_s + 2a\sqrt{\frac{c}{\sigma}}\, B'_{L_t}. \tag{2.5}$$

For every finite $p \geq 1$,

$$\sup_{n\geq 1} \mathbb{E}\left[\left\|h^{-3/4}(X - X^h)\right\|_\infty^p\right] < \infty. \tag{2.6}$$

In particular the squared terminal errors are uniformly integrable. Conditionally on the original path, U_T is centred Gaussian with variance

$$V_T = a\sigma c\left(1 - e^{-4aL_T/\sigma^2}\right), \tag{2.7}$$

and

$$\lim_{n\to\infty} n^{3/2}\mathbb{E}|X_T - X_T^h|^2 = T^{3/2}\mathbb{E}V_T. \tag{2.8}$$

Thus the variance of the limit under $n^{3/4}$, rather than $h^{-3/4}$, is $T^{3/2}V_T$. If $x_0 \neq 0$, paths that do not hit zero contribute a degenerate Gaussian of variance zero.

Proof. Sections 3 and 4 establish the corrector limit, control the endogenous feedback and identify the limiting Volterra equation. They prove the moment bound as well as convergence in law; Section 5 evaluates the remaining local-time expectation. We first work with $T = \sigma = 1$ and restore general parameters at the end of Section 4. □

3. Brownian corrector and quadrature limit

Lemma 1 (Bounded corrector)**.** For a standard Brownian segment B on $[0,1]$ and the centred step function H below, there is a bounded odd solution F of $(I - P_1)F = g$. The centred increment r defined below satisfies $|r| \leq 2$, and its variance and Brownian cross-moment are bounded integrable functions.

Proof. Let P_t be the unit Brownian semigroup and

$$H(x) = \begin{cases} 1 & x > 0, \\ 1/2 & x = 0, \\ 0 & x < 0. \end{cases} \tag{3.1}$$

For a standard Brownian path B on $[0,1]$, define

$$q(x,B) = \int_0^1 \{H(x + B_s) - H(x)\}\, ds, \qquad g(x) = \mathbb{E}q(x,B) = \int_0^1 (P_s H - H)(x)\, ds. \tag{3.2}$$

The function g is bounded, odd and integrable: for $x > 0$, $|g(x)| \le \Phi(-x)$, and the negative half-line follows by symmetry. Define

$$F_N(x) = \sum_{k=0}^{N-1} P_k g(x) = \int_0^N P_t H(x)\, dt - \sum_{k=0}^{N-1} P_k H(x). \tag{3.3}$$

For $x > 0$, the function $t \mapsto P_t H(x)$ decreases from 1 to $1/2$. Each summand in F_N is nonpositive and its absolute value is at most $P_k H(x) - P_{k+1} H(x)$. Consequently F_N converges absolutely pointwise and $|F_N| \le 1/2$. For $x < 0$ use symmetry, and $F_N(0) = 0$. Write its bounded odd limit as F. Since

$$F_N - P_1 F_N = g - P_N g, \tag{3.4}$$

bounded convergence and $\|P_N g\|_\infty \le (2\pi N)^{-1/2} \|g\|_1$ give the pointwise Poisson equation

$$(I - P_1)F = g. \tag{3.5}$$

We also need decay. For $x > 0$, put $f_x(t) = \Phi(x/\sqrt{t})$, with $f_x(0) = 1$. Summing the integral error on each unit interval gives

$$F(x) = \int_0^\infty (1 - \{t\}) f_x'(t)\, dt = -\frac{1}{4} + \int_0^\infty (1/2 - \{t\}) f_x'(t)\, dt. \tag{3.6}$$

The continuous periodic function $A(t) = \frac{1}{2}\{t\}(1 - \{t\})$ is bounded and has derivative $1/2 - \{t\}$ away from integers. Integration by parts, with vanishing boundary terms, gives

$$\left| F(x) + \frac{1}{4} \right| \le \|A\|_\infty \int_0^\infty |f_x''(t)|\, dt = \frac{\|A\|_\infty}{x^2} \int_0^\infty |f_1''(t)|\, dt. \tag{3.7}$$

The last integral is finite: at zero its integrand has Gaussian decay in $1/t$, and at infinity it is $O(t^{-5/2})$. The identity uses $f_x(t) = f_1(t/x^2)$. Oddness proves the corresponding negative-tail estimate. In particular

$$K(x) := F(x) + \tfrac{1}{4} \operatorname{sgn}(x) \ \in L^1(\mathbb{R}) \cap L^2(\mathbb{R}). \tag{3.8}$$

Now set

$$r(x, B) = q(x, B) + F(x + B_1) - F(x), \qquad v(x) = \mathbb{E} r(x, B)^2, \qquad w(x) = \mathbb{E}[r(x, B) B_1]. \tag{3.9}$$

Equation (3.5) gives $\mathbb{E} r(x, B) = 0$ for every x, and $|r| \le 2$. For large $|x|$, $q(x, B)$ vanishes unless the Brownian path crosses $-x$, an event of probability at most $Ce^{-x^2/2}$. On $\{|B_1| \le |x|/2\}$, (3.7) gives $|F(x + B_1) - F(x)| \le C|x|^{-2}$; the complement has Gaussian probability. Thus

$$0 \le v(x) \le \frac{C}{1 + x^4}, \qquad |w(x)| \le \sqrt{v(x)} \le \frac{C}{1 + x^2}. \tag{3.10}$$

Both kernels are bounded and integrable. This also proves the square-integrability needed for the next calculation. □

Use the Fourier convention $\hat{f}(\xi) = \int e^{-i\xi x} f(x)\,dx$. Set $\lambda = \xi^2/2$, $p = e^{-\lambda}$, and

$$D(\xi) = \frac{1}{\lambda} - \frac{1}{1-e^{-\lambda}}. \tag{3.11}$$

The Poisson equation and $\widehat{H'} = 1$ give, for $\xi \neq 0$,

$$\hat{g}(\xi) = \frac{(1-p)/\lambda - 1}{i\xi}, \qquad \widehat{K}(\xi) = \frac{D(\xi) + 1/2}{i\xi}. \tag{3.12}$$

There is no ambiguity at zero: $K \in L^1$ is odd, its transform is continuous with value zero there, and $D(\xi)+1/2 = O(\xi^2)$. Equivalently the transform of F, modulo a constant which cancels under translation, is $D(\xi)/(i\xi)$. Formula (3.8) justifies the use of this identity for $F(\cdot + z) - F$ in L^2; the translated differences of H are in L^2 as well.

Write

$$J = \int_0^1 e^{i\xi B_s}\,ds, \qquad Z = e^{i\xi B_1}, \qquad m = \frac{1-p}{\lambda}. \tag{3.13}$$

Then, almost everywhere in ξ,

$$\widehat{r(\cdot, B)}(\xi) = \frac{J - 1 + D(\xi)(Z-1)}{i\xi}. \tag{3.14}$$

Gaussian increments give

$$\begin{aligned} \mathbb{E}J &= m, & \mathbb{E}Z &= p, \\ \mathbb{E}|J|^2 &= \frac{2}{\lambda} - \frac{2(1-p)}{\lambda^2}, & \mathbb{E}|Z-1|^2 &= 2(1-p), \\ \mathbb{E}[(J-1)\overline{(Z-1)}] &= 1-p. \end{aligned} \tag{3.15}$$

For the last equality, $\mathbb{E}[J\overline{Z}] = m$. Substituting $D = 1/\lambda - 1/(1-p)$ and simplifying therefore gives

$$\mathbb{E}|J - 1 + D(Z-1)|^2 = \frac{1+p}{1-p} - \frac{2}{\lambda} = \coth(\lambda/2) - \frac{2}{\lambda}. \tag{3.16}$$

Plancherel and Tonelli, justified by (3.10), now yield

$$\int_{\mathbb{R}} v(x)\,dx = \frac{1}{\pi}\int_0^\infty \frac{\coth(\xi^2/4) - 4/\xi^2}{\xi^2}\,d\xi. \tag{3.17}$$

The integrand is bounded at zero and $O(\xi^{-2})$ at infinity. With $t = \xi^2/2$, this becomes

$$\frac{1}{\sqrt{2}\pi}\int_0^\infty t^{-3/2}\left(\frac{1}{e^t - 1} - \frac{1}{t} + \frac{1}{2}\right)dt. \tag{3.18}$$

For $-1 < s < 0$, the convergent, subtracted Mellin representation is

$$\Gamma(s)\zeta(s) = \int_0^\infty t^{s-1}\left(\frac{1}{e^t-1} - \frac{1}{t} + \frac{1}{2}\right) dt. \tag{3.19}$$

It follows by splitting the standard Mellin integral at 1, subtracting its two small-t terms and analytically continuing; the added terms on $[1,\infty)$ give $1/(s-1) - 1/(2s)$. Taking $s = -1/2$, with $\Gamma(-1/2) = -2\sqrt{\pi}$, proves

$$\boxed{\int v = c = -\sqrt{2/\pi}\,\zeta(-1/2).} \tag{3.20}$$

The quantity is strictly positive by (3.17). No occupation-time error constant is imported from another paper.

Lemma 2 (Stable quadrature limit)**.** In the normalisation $T = \sigma = 1$, the exact-path drift quadrature Y_n defined below converges stably to $2a\sqrt{c}\,B'_L$. Its supremum norm has bounded moments of every finite order, uniformly in n.

Proof. Only the following specialisations are needed. For clarity, we state the two external limit results in the form used here. ***Occupation law [5].*** *If $Y = x + B$ is unit Brownian motion and f is bounded, Borel and integrable, then for $u_n \to \infty$, $u_n/n \to 0$,*

$$\frac{u_n}{n}\sum_{k<nt} f(u_n Y_{k/n}) \xrightarrow{\text{ucp}} L_t^0(Y)\int_{\mathbb{R}} f(y)\,dy. \tag{3.21}$$

Here and below $k < nt$ in sums means $k = 0, \dots, \lfloor nt \rfloor - 1$. This is [5, Thm. 1.1], with its two-variable function independent of the increment variable. Hypothesis B-0 is precisely supplied by boundedness and integrability; condition (1.11) is $u_n/n \to 0$, not $u_n/\sqrt{n} \to 0$. The local-time convention in that paper's equation (1.2) is the one above. In particular both $u_n = \sqrt{n}$ and $u_n = n^{3/4}$ are permitted. Convergence in probability transfers to an equivalent probability measure on a fixed horizon. ***Discrete martingale CLT [6].*** *In the completed natural Brownian filtration, a square-integrable triangular array of martingale differences has a stable continuous conditional-Gaussian limit if its predictable variance converges to a continuous adapted increasing process, its predictable covariation with the Brownian increments tends to zero, and conditional Lindeberg holds. This is the zero-drift, zero-cross-covariance specialisation of [6, Thm. 3-2], conditions (3.10)–(3.14). The condition involving bounded martingales orthogonal to the basic Brownian motion is automatic in its natural filtration, by martingale representation. The theorem applies to the discretised filtration; it does not require the step processes to be martingales in the full continuous-time filtration. First work under a measure Q where $Y_t = x_0 + B_t$ is Brownian. Define*

$$A_n(t) = n^{3/4}\int_0^t [H(Y_s) - H(Y_{\lfloor ns\rfloor/n})]ds, \quad x_{n,k} = \sqrt{n}\,Y_{k/n}, \quad B_s^{n,k} = \sqrt{n}(B_{(k+s)/n} - B_{k/n}). \tag{3.22}$$

At grid points, $A_n = n^{-1/4} \sum q(x_{n,k}, B^{n,k})$. *The array*

$$M_n(t) = n^{-1/4} \sum_{k<nt} r(x_{n,k}, B^{n,k}) \tag{3.23}$$

is a martingale in the discretised filtration. The correction telescopes and the incomplete final interval contributes at most $n^{-1/4}$, *so*

$$\|A_n - M_n\|_\infty \le 2n^{-1/4}. \tag{3.24}$$

Its predictable variance is

$$\langle M_n \rangle_t = n^{-1/2} \sum_{k<nt} v(\sqrt{n} Y_{k/n}) \xrightarrow{\text{ucp}} c L_t^0(Y) \tag{3.25}$$

by (3.21) *and* (3.20). *Its predictable covariation with the grid Brownian increments is*

$$n^{-3/4} \sum_{k<nt} w(\sqrt{n} Y_{k/n}). \tag{3.26}$$

The absolute value uniformly in time is bounded by

$$n^{-1/4} \left[n^{-1/2} \sum_{k<n} |w(\sqrt{n} Y_{k/n})| \right] \xrightarrow{Q} 0 \tag{3.27}$$

using (3.21) *and* (3.10). *Finally* $|\Delta M_n| \le 2n^{-1/4}$, *so conditional Lindeberg holds identically for sufficiently large* n. *The discrete CLT stated above proves*

$$A_n \Longrightarrow_{\text{st}} \sqrt{c}\, B'_{L^0(Y)}. \tag{3.28}$$

The limit is continuous, and (3.24) *transfers the convergence from the step martingales to the continuous processes in the uniform topology. Here are moment bounds, needed independently of the CLT. Under* Q, *the chain* $x_{n,k}$ *has unit normal increments, starting at* $\sqrt{n} x_0$. *For* $V = \|v\|_\infty$,

$$\sup_x \mathbb{E}_x \sum_{k=0}^{n-1} v(x + B_k) \le V + \frac{\|v\|_1}{\sqrt{2\pi}} \sum_{k=1}^{n-1} k^{-1/2} \le C\sqrt{n}. \tag{3.29}$$

Expanding integer moments of this nonnegative sum, ordering the indices and using the Markov property recursively gives

$$\sup_x \mathbb{E}_x \left(\sum_{k=0}^{n-1} v(x + B_k) \right)^m \le m! C_m n^{m/2}, \qquad m \in \mathbb{N}. \tag{3.30}$$

For completeness, repeated indices can be removed with $v^j \le V^{j-1} v$; *for* ℓ *distinct ordered indices the sum of expected products is at most* $(C\sqrt{n})^\ell$ *by* (3.29). *Summing over the finitely many compositions of* m *proves* (3.30), *with a constant depending only on* m *and* v. *Apply the discrete Burkholder–Rosenthal maximal inequality at exponent* $2m$. *The*

predictable-variance term is bounded by (3.30). The remaining term satisfies

$$\sum_{k<n} \mathbb{E}_Q |\Delta M_{n,k}|^{2m} \le 2^{2m-2} n^{-m/2} \sum_{k<n} \mathbb{E}_Q v(x_{n,k}) \le C_m n^{(1-m)/2} \le C_m. \tag{3.31}$$

Thus $\sup_n \mathbb{E}_Q \|M_n\|_\infty^{2m} < \infty$, *and (3.24) and interpolation give*

$$\sup_n \mathbb{E}_Q \|A_n\|_\infty^p < \infty \qquad \text{for every finite } p \ge 1. \tag{3.32}$$

Now let X be the unit-diffusion sign-drift solution under the original measure P. Boundedness of the drift allows an equivalent measure Q under which $X = x_0 + B$ on $[0,1]$. Conversely

$$Z := \frac{dP}{dQ} = \exp\left(-a \int_0^1 \operatorname{sgn}(X_s) dB_s - \frac{a^2}{2} \int_0^1 \operatorname{sgn}(X_s)^2 ds \right). \tag{3.33}$$

For every $r > 1$, $\mathbb{E}_Q Z^r \le \exp((r^2 - r)a^2/2)$. The filtration is the natural filtration of X, which is also that of the driving Brownian motion under either measure: one direction follows from strong solvability and the other from recovering the driving path from X. Stable convergence transfers from Q to P by multiplying test variables by Z and truncating Z in $L^1(Q)$. The independent conditional-Gaussian kernel is unchanged; only the distribution of the base path changes. Hölder's inequality and (3.32), with exponent $2p$, transfer the uniform p-moment bound as well. Since $-a \operatorname{sgn} = -2aH + a$, the exact-path drift quadrature

$$Q_n(t) = \int_0^t [b(X_s) - b(X_{\lfloor ns \rfloor / n})] ds, \qquad b = -a \operatorname{sgn}, \tag{3.34}$$

therefore satisfies, under P,

$$Y_n := n^{3/4} Q_n \Longrightarrow_{\text{st}} 2a\sqrt{c}\, B'_L, \qquad \sup_n \mathbb{E} \|Y_n\|_\infty^p < \infty. \tag{3.35}$$

The harmless minus sign is absorbed into B'. □

4. Local-time feedback and identification

Lemma 3 (Endogenous local-time feedback)**.** In the same normalisation, put $U_n = n^{3/4}(X - X^{1/n})$. Then U_n is C-tight with bounded supremum moments of every finite order. If D_n denotes the drift feedback below, then $n^{3/4} D_n + 2a \int_0^{\cdot} U_n \, dL$ converges uniformly in probability to zero.

Proof. Put $e_n = X - X^{1/n}$. Cancellation of the common driving noise gives the exact decomposition

$$e_n(t) = Q_n(t) + D_n(t), \qquad D_n(t) = \int_0^t f_{n,k}(e_n(k/n)) ds \quad (k = \lfloor ns \rfloor), \tag{4.1}$$

where

$$f_{n,k}(z) = b(X_{k/n}) - b(X_{k/n} - z). \tag{4.2}$$

Because b is nonincreasing,

$$z f_{n,k}(z) \le 0, \qquad |f_{n,k}(z)| \le 2a. \tag{4.3}$$

Let $d = \|Q_n\|_\infty$. At a grid point, if $D_n(k/n) > d$, then $e_n(k/n) > 0$, so the next increment of D_n is nonpositive. If $D_n(k/n) \le d$, an upward increment is at most $2a/n$. The analogous lower bound and induction from zero show

$$|D_n(k/n)| \le d + 2a/n. \tag{4.4}$$

Between grid points D_n is linear, so this bound holds throughout the interval. Hence

$$\boxed{\|e_n\|_\infty \le 2\|Q_n\|_\infty + 2a/n.} \tag{4.5}$$

This handles discrete overshoots; no Lipschitz derivative of the sign function is assumed. By (3.35),

$$U_n := n^{3/4} e_n, \qquad \sup_n \mathbb{E}\|U_n\|_\infty^p < \infty \tag{4.6}$$

for all finite p. We next prove C-tightness, rather than assuming it in the feedback argument. On $\{\|U_n\|_\infty \le R\}$, a nonzero $f_{n,k}(e_n(k/n))$ requires $|X_{k/n}| \le R n^{-3/4}$. By (3.21),

$$J_{n,R}(t) := n^{-1/4} \sum_{k<nt} \mathbf{1}_{\{|n^{3/4} X_{k/n}| \le R\}} \xrightarrow{\text{ucp}} 2RL_t. \tag{4.7}$$

On this event the variation of $n^{3/4} D_n$ over $[s,t]$ is bounded by

$$2a\{J_{n,R}(t) - J_{n,R}(s) + 2n^{-1/4}\}. \tag{4.8}$$

The right-hand side has a continuous limiting modulus because L is continuous. The probability of the complementary event can be made arbitrarily small uniformly in n using (4.6). Thus $n^{3/4} D_n$ is C-tight, and so is $U_n = Y_n + n^{3/4} D_n$ by (3.35). For $u, y \in \mathbb{R}$, write

$$G(u,y) = H(y) - H(y-u). \tag{4.9}$$

For fixed u, this is bounded, integrable and has integral u. For fixed y it is nondecreasing in u, including when $u < 0$; its endpoint values are fixed by $H(0) = 1/2$. Define

$$C_n(t,u) = n^{-1/4} \sum_{k<nt} G(u, n^{3/4} X_{k/n}). \tag{4.10}$$

By (3.21), $C_n(\cdot, u) \to uL$ uniformly in probability for each fixed u. Monotonicity in u, a finite mesh of $[-R,R]$, and continuity of $u \mapsto uL_t$ imply

$$\delta_{n,R} := \sup_{t \le 1,\, |u| \le R} |C_n(t,u) - uL_t| \xrightarrow{P} 0. \tag{4.11}$$

Indeed a spatial mesh of width ε bounds the displayed supremum by the largest error at its finitely many mesh points plus εL_1. We claim that for any C-tight continuous processes Z_n,

$$\sup_{t\le 1}\left|n^{-1/4}\sum_{k<nt} G(Z_n(k/n), n^{3/4}X_{k/n}) - \int_0^t Z_n(s)dL_s\right| \xrightarrow{P} 0. \tag{4.12}$$

This statement permits complete dependence of Z_n on the observed path. To prove it, restrict first to $\|Z_n\|_\infty \le R$ and $L_1 \le K$. On a deterministic time partition with mesh at most δ, restrict further to the event that Z_n oscillates by at most ε within each block (allowing an extra grid step). Freeze its value at each block's left endpoint. Monotonicity of G sandwiches the true block sum between frozen sums evaluated at the frozen value minus and plus ε. Formula (4.11), uniformly in the possibly random frozen value, identifies each of those sums up to $2\delta_{n,R+1}$ with that frozen value times the increment of L. The integral of Z_n differs from its frozen counterpart by at most ε times that increment of L. For a partition with m blocks the total error, uniformly over terminal times, is therefore at most

$$2\varepsilon K + 2m\delta_{n,R+1} + Cmn^{-1/4}. \tag{4.13}$$

The last term accounts for grid endpoints and a last partial block; $|G| \le 1$. First send $n \to \infty$ at fixed partition. C-tightness permits $\delta \downarrow 0$ so that the oscillation event has arbitrarily high probability. Then send $\varepsilon \downarrow 0$, and finally remove the bounds R, K using tightness. This proves (4.12). Apply (4.12) to $Z_n = U_n$, whose C-tightness was proved in the preceding stability argument. Homogeneity of the sign function gives exactly

$$n^{3/4}D_n(t) = -2an^{-1/4}\sum_{k<nt} G(U_n(k/n), n^{3/4}X_{k/n}) + O(n^{-1/4}), \tag{4.14}$$

where the error is bounded uniformly by $2an^{-1/4}$. Consequently

$$\left\|n^{3/4}D_n + 2a\int_0^{\cdot} U_n(s)dL_s\right\|_\infty \xrightarrow{P} 0. \tag{4.15}$$

This is the required random-boundary feedback result; no independence or unproved substitution of a random threshold into a pointwise occupation limit is used. □

Combining the exact decomposition with (4.15) gives

$$U_n(t) = Y_n(t) - 2a\int_0^t U_n(s)dL_s + R_n(t), \qquad \|R_n\|_\infty \xrightarrow{P} 0. \tag{4.16}$$

For continuous y with $y(0) = 0$ and continuous nondecreasing ℓ with $\ell(0) = 0$, the unique solution of

$$u(t) = y(t) - 2a\int_0^t u(s)d\ell_s \tag{4.17}$$

is the pathwise map

$$\mathcal{S}(y,\ell)(t) = y(t) - 2ae^{-2a\ell_t}\int_0^t e^{2a\ell_s}y(s)d\ell_s. \tag{4.18}$$

This follows directly by solving the finite-variation equation for $u-y$. Its operator norm in y, for a fixed ℓ, is at most 2, since $2ae^{-2a\ell_t}\int_0^t e^{2a\ell_s}d\ell_s = 1-e^{-2a\ell_t} \le 1$. It is jointly continuous for uniform convergence of y,ℓ, with ℓ restricted to continuous nondecreasing paths: the associated Stieltjes measures converge weakly and their total masses stay bounded. Continuity of the limit integrands and partition approximation make the convergence uniform in the upper endpoint.

Equation (4.16) therefore implies

$$\|U_n - \mathcal{S}(Y_n, L)\|_\infty \le 2\|R_n\|_\infty \xrightarrow{P} 0. \tag{4.19}$$

The stable continuous-mapping theorem, (3.35), and joint convergence with the fixed base-path variable L prove (2.4)–(2.5) for $T=\sigma=1$. The stochastic-integral representation of the limit is

$$U_t = 2a\sqrt{c}\,e^{-2aL_t}\int_0^t e^{2aL_s}\,dB'_{L_s}. \tag{4.20}$$

Conditioning on the original path and using the Itô isometry gives

$$\mathrm{Var}(U_t \mid X) = 4a^2c\,e^{-4aL_t}\int_0^t e^{4aL_s}dL_s = ac(1-e^{-4aL_t}). \tag{4.21}$$

The uniform moment bound (4.6), at any exponent strictly larger than 2, proves uniform integrability of $U_n(1)^2$. Hence convergence in distribution now legitimately yields convergence of the second moments. This proves (2.6)–(2.8) in the normalised case.

If the original probability space has additional randomness, the stable statement extends from the Brownian path sigma-field to the terminal sigma-field by conditional projection of any bounded test variable onto the Brownian path: every prelimit error and the limiting conditional law are functions of that path.

Set

$$\widetilde{X}_s = \frac{X_{Ts}}{\sigma\sqrt{T}}, \qquad \alpha = \frac{a\sqrt{T}}{\sigma}, \qquad \tilde{x}_0 = \frac{x_0}{\sigma\sqrt{T}}. \tag{4.22}$$

Then $d\widetilde{X} = -\alpha\,\mathrm{sgn}(\widetilde{X})ds + d\widetilde{W}_s$, its Euler grid is $1/n$, and

$$L^0_s(\widetilde{X}) = \frac{L^0_{Ts}(X)}{\sigma\sqrt{T}}, \qquad h^{-3/4}(X_{Ts} - X^h_{Ts}) = \sigma T^{-1/4}n^{3/4}(\widetilde{X}_s - \widetilde{X}^{1/n}_s). \tag{4.23}$$

Applying the normalised theorem and Brownian scaling on the independent extension gives exactly (2.4)–(2.8), including the factor $T^{3/2}$ in the n-normalised MSE.

5. Explicit mean-square constant

Corollary 1 (Closed terminal constant)**.** Let $r = a\sqrt{T}/\sigma$ and $z = |x_0|/(\sigma\sqrt{T})$. With Φ the standard normal distribution function, define

$$\Psi(z, r) = \Phi(z - r) - 2e^{2rz}\Phi(-z - r) + 3e^{4rz+4r^2}\Phi(-z - 3r). \tag{5.1}$$

The limit of $n^{3/2}\mathbb{E}|X_T - X_T^{T/n}|^2$ is

$$C(a, \sigma, T, x_0) = T^{3/2}a\sigma c[1 - \Psi(z, r)]. \tag{5.2}$$

Proof. Tanaka's formula gives

$$|X_t| = |x_0| - at + \sigma\beta_t + L_t, \tag{5.3}$$

where $\beta = \int \operatorname{sgn}(X)dW$ is a standard Brownian motion: the set $\{X = 0\}$ has zero Lebesgue time, by the occupation formula. The increasing process L only grows at zero. Uniqueness of the one-dimensional Skorokhod reflection map therefore gives the distributional identity

$$L_T \overset{d}{=} \sigma(M_T - d)_+, \quad M_T = \sup_{s\le T}(B_s + \mu s), \quad \mu = a/\sigma, \quad d = |x_0|/\sigma. \tag{5.4}$$

Reflection with drift yields, for $m \ge 0$,

$$\mathbb{P}(M_T \le m) = \Phi\left(\frac{m - \mu T}{\sqrt{T}}\right) - e^{2\mu m}\Phi\left(\frac{-m - \mu T}{\sqrt{T}}\right). \tag{5.5}$$

Put $r = a\sqrt{T}/\sigma$ and $z = |x_0|/(\sigma\sqrt{T})$. Integrating (5.5) against $4\mu e^{-4\mu l}dl$, with argument $m = d + l$, gives

$$\Psi(z, r) := \mathbb{E}e^{-4aL_T/\sigma^2} = \Phi(z - r) - 2e^{2rz}\Phi(-z - r) + 3e^{4rz+4r^2}\Phi(-z - 3r). \tag{5.6}$$

This calculation includes the atom $L_T = 0$, since for any nonnegative V, $\mathbb{E}e^{-qV} = q\int_0^\infty e^{-ql}\mathbb{P}(V \le l)dl$. To check the coefficients, integration by parts in the first CDF term produces $\Phi(z - r) + e^{4rz+4r^2}\Phi(-z - 3r)$; the second produces $2e^{2rz}\Phi(-z - r) - 2e^{4rz+4r^2}\Phi(-z - 3r)$, which is subtracted. Thus the fully explicit constant for every deterministic starting point is

$$\boxed{\lim_{n\to\infty} n^{3/2}\mathbb{E}|X_T - X_T^h|^2 = T^{3/2}a\sigma c[1 - \Psi(z, r)].} \tag{5.7}$$

In particular, for $x_0 = 0$,

$$\boxed{T^{3/2}a\sigma c\,[1 + \Phi(-r) - 3e^{4r^2}\Phi(-3r)].} \tag{5.8}$$

□

6. Dry friction and time-step selection

In the pure dry-friction model [8], X is velocity, a is the magnitude of the frictional acceleration, and σ is the intensity of the random acceleration. Friction reverses direction when velocity crosses zero. The theorem concerns this model with Gaussian white noise, constant coefficients, no viscous drag and no additional constant force. It does not assert a result for a deterministic sticking interval or for a model with a static-friction threshold.

For a fixed physical horizon T, the relevant simulation error is

$$\mathrm{RMSE}(n) = \left(\mathbb{E}|X_T - X_T^{T/n}|^2\right)^{1/2} \sim \sqrt{C}\, n^{-3/4}. \tag{6.1}$$

Thus a target terminal velocity tolerance $\varepsilon > 0$ suggests

$$n_{\mathrm{asy}} = \max\{1, \lceil (C/\varepsilon^2)^{2/3} \rceil\}, \qquad h_{\mathrm{asy}} = T/n_{\mathrm{asy}}. \tag{6.2}$$

For nested Brownian coupling it is convenient to round this number upward to a power of two. This is a starting prescription, not a finite-mesh upper bound: the theorem gives an asymptotic equivalent and does not supply a remainder estimate. The numerical check must therefore compare the selected mesh with finer coupled references and record both Monte Carlo uncertainty and reference sensitivity.

The local-time factor explains why this model needs a different error assessment from a smooth restoring force. The leading error accumulates at zero velocity, while the inward drift damps the already accumulated error through the same local time. The terminal variance saturates at $a\sigma c$ in the $h^{-3/4}$ normalisation. This describes discretisation error under the same driving noise; it is distinct from uncertainty in the physical forcing or in estimated model parameters.

Algorithm 1 — Mesh selection for terminal velocity error

Inputs: $a, \sigma, T > 0$, deterministic initial velocity x_0, target RMS tolerance ε, and a Monte Carlo path budget M.

1. Evaluate C from Corollary 1, using log-CDF expressions for exponential-tail products; for a small tail probability, evaluate the corresponding nonnegative Brownian-maximum survival integral to avoid subtractive cancellation.
2. Form n_{asy} and round upward to a dyadic mesh n.
3. Couple the selected Euler mesh and two finer references with common Brownian increments; save the paths and seeds once.
4. Report RMS error against each reference, sampling uncertainty and observed order across available meshes.
5. Accept the mesh only to the extent supported by these diagnostics; refine if the target or reference check is unresolved.

Cost: $O(MN)$ operations for a fixed number of meshes and reference size N; paths can be streamed with $O(N)$ storage per worker. The present study reuses saved simulations.

All reported experiments use $T = \sigma = 1$, $x_0 = 0$, and $a = 1$ or $a = 2$. Each case has 8,192 independent paths, a 524,288-step Euler reference and a paired 262,144-step reference. Brownian increments are nested; deterministic seeds are 771026 and 871026, incremented by the path index. We reuse these saved paths and their established summary statistics.

The closed constants are $C = 0.1555105857$ and $C = 0.3305605321$. Independently of Euler simulation, the Fourier integral gives $c = 0.165869209312827$, agreeing with the zeta expression within 2×10^{-13}. An exact Gaussian arcsine calculation for Brownian occupation gives a scaled error of 0.1323405203 at 2,048 intervals, approaching $c\sqrt{2/\pi} = 0.1323444812$. Three parameter sets check the local-time Laplace formula against integration of the Brownian-maximum distribution to absolute error below 3×10^{-15}.

The first table reports $S_n = n^{3/2}\widehat{\mathbb{E}}|X_T^N - X_T^n|^2$, its Monte Carlo standard error, and the observed RMS order between displayed meshes. Reference sensitivity is the signed change in S_n when the finer reference replaces the coarser one. It is a diagnostic, not a bound on reference bias. At the finest displayed mesh the scaled errors remain above their theoretical limits, so these samples are not presented as a high-precision numerical confirmation of the constants.

For the tolerance table, we apply Algorithm 1 to targets 0.002, 0.001 and 0.0005. The intervals use the delta method for Monte Carlo uncertainty in RMS error; they do not include reference bias. This distinction is material for the $a = 2$, 0.002 target, whose selected mesh sits near the tolerance. As emphasized in [9], finite-grid reference experiments measure a coupled approximation error, not error against an observed exact solution.

The borderline case also illustrates the refinement step: keeping $a = 2$ and the target 0.002, the already available 4,096-step mesh gives RMS/target 0.581, with Monte Carlo interval [0.572, 0.590]. This resolves the sampling comparison against the selected reference while retaining the reference-bias qualification.

Euler error in the dry-friction model

8,192 paths per regime; reference N = 524,288; paired reference N/2

a	Steps n	Scaled MSE	MC s.e.	RMS order	Ref. change
1	1,024	0.165197	0.002645	-	-0.000019
1	4,096	0.164648	0.002582	0.751	-0.000023
1	16,384	0.162210	0.002570	0.755	+0.001238
2	1,024	0.384899	0.005905	-	+0.000256
2	4,096	0.354279	0.005704	0.780	+0.000059
2	16,384	0.339391	0.005403	0.765	+0.001361

Limits: a = 1: 0.155510586; a = 2: 0.330560532. RMS order uses successive displayed meshes.
Reference change is signed (N minus N/2); it does not bound the remaining reference bias.

Figure 1: Scaled terminal mean-square errors for the two dry-friction regimes, with Monte Carlo standard errors, observed RMS orders and signed reference-grid changes.

The observed order is $p = 3/4 + \log(S_{n_1}/S_{n_2})/[2\log(n_2/n_1)]$. The exact constants are the limits of the scaled column; neither the standard error nor the reference change alone accounts for all finite-mesh bias.

Selecting a mesh for a velocity-error tolerance

Dimensionless examples: sigma = T = 1, initial velocity = 0; same saved coupling experiment

a	RMS target	Asymptotic n	Dyadic n	RMS / target	95% MC interval
1	0.0020	1,148	2,048	0.668	[0.658, 0.679]
1	0.0010	2,892	4,096	0.793	[0.780, 0.805]
1	0.0005	7,287	8,192	0.941	[0.926, 0.955]
2	0.0020	1,898	2,048	0.991	[0.976, 1.006]
2	0.0010	4,781	8,192	0.683	[0.673, 0.694]
2	0.0005	12,047	16,384	0.805	[0.792, 0.817]

Intervals describe Monte Carlo uncertainty in RMS/target; they exclude reference and model error.
The a = 2, target = 0.002 interval reaches 1: this target remains unresolved at the stated precision.

Figure 2: Asymptotic mesh choices and measured terminal RMS errors for three prescribed tolerances in each dry-friction regime, using saved coupled paths.

An upper Monte Carlo endpoint below one supports the tolerance only relative to the chosen numerical reference. An interval reaching one leaves the target unresolved at that sampling precision; a finer reference is not an exact path.

7. Conclusion

For inward sign drift, Euler error has a local-time-driven Gaussian limit with local-time damping. The bounded corrector identifies its universal constant, the shrinking-band lemma handles the endogenous feedback, and moment bounds justify an exact mean-square asymptotic. Reflection converts the remaining local-time expectation to normal CDFs for any deterministic initial value.

The dry-friction application turns that constant into a mesh-selection rule and an explicit accuracy check. The rule is asymptotic, and the supplied simulations preserve the distinction between Monte Carlo uncertainty, finite-grid effects and reference error. Extensions to viscous friction, several discontinuities or adaptive meshes require additional analysis.

References

[1] Neuenkirch, Andreas, & Szölgyenyi, Michaela (2020). The Euler–Maruyama scheme for SDEs with irregular drift: convergence rates via reduction to a quadrature problem. *IMA Journal of Numerical Analysis*. https://doi.org/10.1093/imanum/draa007

[2] Müller-Gronbach, Thomas, & Yaroslavtseva, Larisa (2023). Sharp lower error bounds for strong approximation of SDEs with discontinuous drift coefficient by coupling of noise. *The Annals of Applied Probability*. https://doi.org/10.1214/22-AAP1837

[3] Ellinger, Simon (2023). Sharp lower error bounds for strong approximation of SDEs with piecewise Lipschitz continuous drift coefficient. *arXiv*. arXiv:2303.05346

[4] Dareiotis, Konstantinos, Gerencsér, Máté, & Lê, Khoa (2026). A central limit theorem for the Euler method for SDEs with irregular drifts. *Stochastics and Partial Differential Equations: Analysis and Computations*. https://doi.org/10.1007/s40072-026-00411-5

[5] JACOD, J (1998). Rates of convergence to the local time of a diffusion. *Annales de l'Institut Henri Poincare (B) Probability and Statistics*. https://doi.org/10.1016/S0246-0203(98)80026-5

[6] Jacod, Jean (1997). On continuous conditional Gaussian martingales and stable convergence in law. *Lecture Notes in Mathematics*. https://doi.org/10.1007/BFb0119308

[7] Altmeyer, Randolf, & Le Guével, Ronan (2022). Optimal L2-approximation of occupation and local times for symmetric stable processes. *Electronic Journal of Statistics*. https://doi.org/10.1214/22-EJS2013

[8] Touchette, Hugo, Van der Straeten, Erik, & Just, Wolfram (2010). Brownian motion with dry friction: Fokker–Planck approach. *Journal of Physics A: Mathematical and Theoretical*. https://doi.org/10.1088/1751-8113/43/44/445002

[9] Göttlich, S., Lux, K., & Neuenkirch, A. (2019). The Euler scheme for stochastic differential equations with discontinuous drift coefficient: a numerical study of the convergence rate. *Advances in Difference Equations*. https://doi.org/10.1186/s13662-019-2361-4

Zamrik Quant Research
The research arm of Zamrik Quant Lab

About the Desk

Stochastic Analysis Desk

Zamrik Quant Research

How random processes behave — Itô calculus, diffusions, local time, Fokker–Planck — in theory and in application.

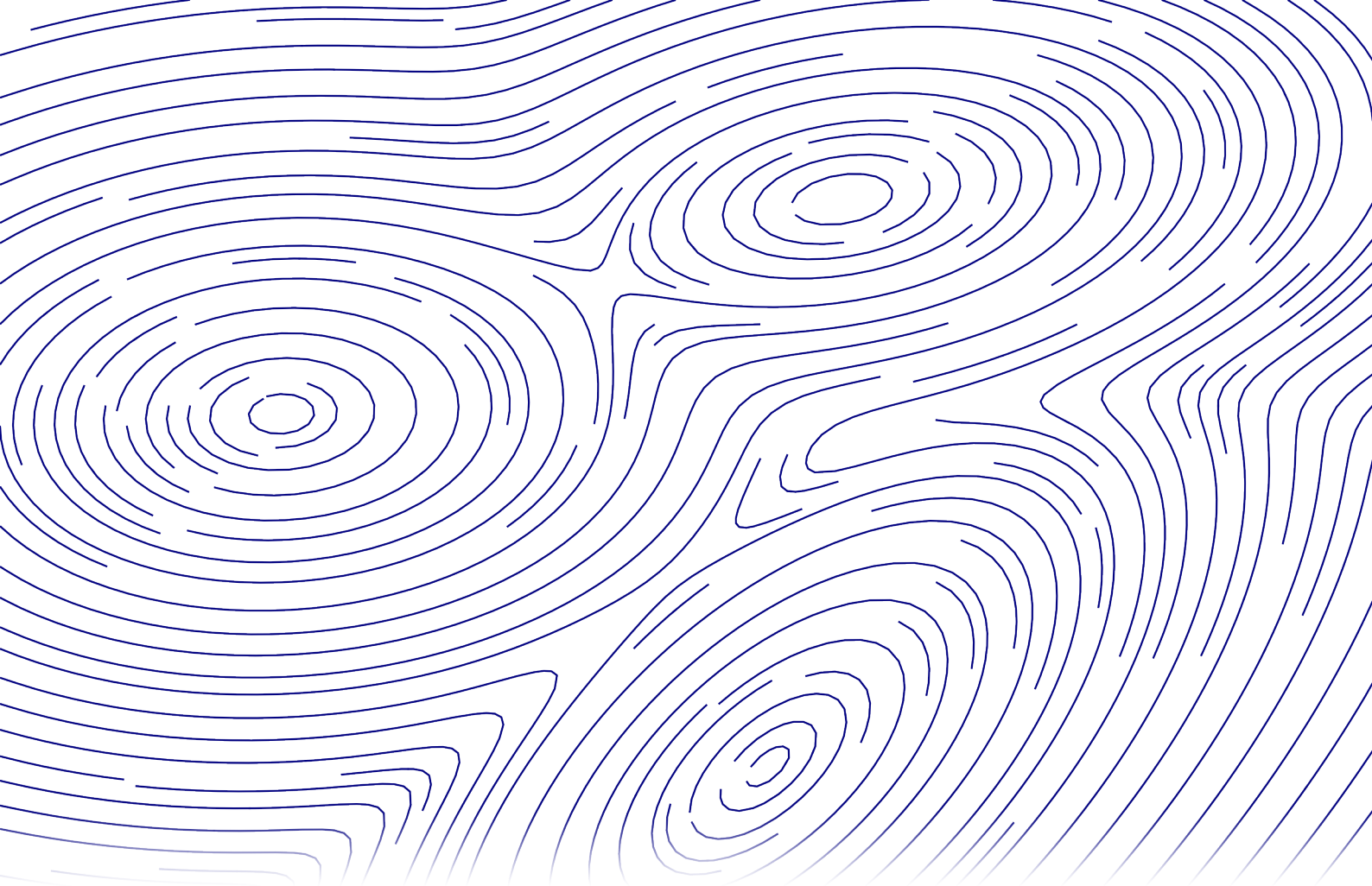
Stochastic analysis is the grammar of every other desk: a price, an order queue, a population or a value function is a functional of a random path, and what can be said about it depends on what can be proved about the path. The Stochastic Analysis desk works on those proofs and on the exact formulas they produce.

Its core questions are the classical ones, asked with care: when a diffusion first reaches a boundary, fixed or moving; how long it spends at each level before it does; and what happens at the boundary itself — reflection, killing, a sticky or skewed point, a reset to the start. The answers come through Itô calculus and martingale methods, local time and Tanaka's formula, Ray–Knight theorems, time changes, and the Feynman–Kac and Fokker–Planck equations that turn questions about paths into equations for expectations and densities. Wherever the problem allows, the desk derives the law in closed form and then checks it against an independently built simulation.

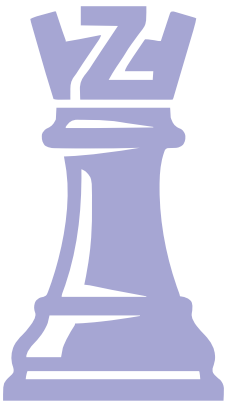
The results travel. The same calculus corrects a barrier that is checked once a day, explains why most stocks lose to the average stock, separates real correlation from the noise of random matrices, sets the acceptance rate of a Metropolis sampler, and models a neuron's membrane and a day's rainfall. The desk also studies the numerics that decide whether a simulated path tells the truth: the strong and weak convergence of Euler–Maruyama and Milstein schemes, Brownian-bridge corrections for barriers monitored in discrete time, and the error left when a continuous process is sampled on a grid.

The desk is supervised by **Dr. T. Zamrik**, Head of Zamrik Quant Research, PhD, Imperial College London (2011).

Notes



Hamiltonian flow of the Gaussian mixture: $\dot{\mathbf{x}} = J\,\nabla f(\mathbf{x}),\ J = \left(\begin{smallmatrix} 0 & -1 \\ 1 & 0 \end{smallmatrix}\right), \quad f(x,y) = \sum_{i=1}^{n} w_i\,\mathcal{N}(x,y;\,\mu_i,\,\Sigma_i)$



ZAMRIK QUANT RESEARCH

The research arm of Zamrik Quant Lab



TN-2026-63585804
zamrik.com